

---

## **The Ohio State University Research**

The following report from Ohio State University for the period contains these brief chapters:

### **Highlights**

#### **Work Performed**

- 1. Development of Fiber Optic Probe System**
- 2. Effect of Pressure on the Gas Holdup of Slurry Bubble Column**

# INTRINSIC FLOW BEHAVIOR IN A SLURRY BUBBLE COLUMN UNDER HIGH PRESSURE AND HIGH TEMPERATURE CONDITIONS

(Reporting Period: October 1 to December 31, 1997)

## Highlights

1. A computer code was developed to process the light intensity signals from a fiber optic probe. The computer code can calculate the bubble rise velocity and bubble chord length distribution from the signals.
2. It was proven in experiments that the probe system and the computer code can be used to measure the bubble size distribution in a slurry bubble column under high-pressure, high-temperature, and high-gas velocity conditions.
3. A new technique was established to measure gas holdup in slurry bubble columns. The new technique has two major advantages over other techniques: elimination of uncertain particle density from the measurement and the capability to determine if the particles are completely suspended.

## Work Performed

### 1. Development of Fiber Optic Probe System

In the last quarter, a dual-tip optical fiber probe was developed to measure bubble size distribution in high-pressure slurry bubble columns. Calibration of the probe proved that the probe system can satisfactorily measure the bubble rise velocity and bubble chord length, provided that the signal from the probe is processed appropriately.

A computer code was developed during this quarter to analyze light intensity signals. The computer code first normalizes the signals based on the following formula:

$$\begin{cases} I_n(t) = 0 & \text{if } I(t) \leq T \\ I_n(t) = 1 & \text{if } I(t) \geq T \end{cases} \quad (1)$$

where  $I_n(t)$  is the normalized light intensity;  $I(t)$  is the original light intensity; and  $T$  is a threshold value.  $T$  is taken as the maximum value in signals from a gas-free liquid-solid suspension. Then a peak in the lower tip signal is used as a trigger to match a peak in the upper tip signal. The  $\Delta t_2$  of these two peaks, shown in Figure 1, should be smaller than 0.018 second, since the detectable minimum bubble rise velocity is 8 cm/s. Also, the ratio of the width of peak ( $\tau$ ) in the upper tip signal to that in the lower tip signal is between 0.7 and 1, based on a calibration. After the peaks are matched, the bubble rise velocity is:

$$U_b = \frac{\Delta L}{\Delta \tau_2} \quad (2)$$

where  $\Delta L$  is the vertical distance between the two measuring tips. The bubble chord length is then

$$l = \tau U_b \quad (3)$$

The computer code was used to analyze the signal when the probe was placed in a chain of bubbles. The result from the computer program matched well that from visualization.

The computer code was then used to analyze the signals obtained from slurry bubble columns. Figure 2 shows a typical signal obtained in a slurry bubble column. The probability density function of the bubble chord length is shown in Figure 3. It can be seen from Figure 3 that the bubble size distribution at the ambient pressure was wide, with a maximum bubble chord length of 6 cm which was more than half of the column size (10.16 cm). This result proves that the bubble column is in the slugging regime at a gas velocity of 34.6 cm/s and at 0.1 MPa pressure.

The computer code will be used to analyze the bubble size distribution and operating regime in slurry bubble columns under high-pressure and high-gas velocity conditions.

## 2. Effect of Pressure on the Gas Holdup of Slurry Bubble Column

With the probe system developed during the past two quarters, attention has shifted to investigating the effect of pressure on the hydrodynamics, including gas holdup and bubble size distribution, in high-pressure slurry bubble columns at high gas velocities.

The measurement of the gas holdup is based on the bed collapse technique described in the quarterly report of July 1997. Efforts were made to further improve that technique, which involves the simultaneous shutdown of both the inlet and outlet of the slurry bubble column after it reaches a steady state. The dynamic pressure gradient signal was recorded with a computer data acquisition system during the entire bed collapse process. The ratio of solids holdup to liquid holdup,  $K$ , in a slurry bubble column at steady state can be calculated from the dynamic pressure drop in the gas-free suspension stage:

$$K = \frac{\epsilon_s^0}{\epsilon_l^0} = \frac{(\Delta P / \Delta z)_d^0}{(\rho_s - \rho_l)g - (\Delta P / \Delta z)_d^0} \quad (4)$$

where  $\epsilon_s^0$ ,  $\epsilon_l^0$ , and  $(\Delta P / \Delta z)_d^0$  are the solids holdup, liquid holdup, and dynamic pressure gradient at the gas-free suspension stage, respectively. At a steady state, the gas holdup can be related to the dynamic pressure gradient, phase densities, and the constant  $K$  by

$$\begin{aligned} \left( \frac{\Delta P}{\Delta z} \right)_d &= (\rho_g \epsilon_g + \rho_l \epsilon_l + \rho_s \epsilon_s - \rho_l)g \\ &= \left\{ \frac{K(\rho_s - \rho_l)}{1+K} + \left[ \frac{(1+K)\rho_g - (\rho_l + K\rho_s)}{1+K} \right] \epsilon_g \right\} g \end{aligned} \quad (5)$$

where  $\epsilon_s$ ,  $\epsilon_l$ ,  $\epsilon_g$ , and  $(\Delta P / \Delta z)_d$  are the solids holdup, liquid holdup, gas holdup, and dynamic pressure gradient at the steady state, respectively. Substituting Eq.(4) into Eq.(5), the gas holdup at the steady state can be derived as

$$\epsilon_g = \frac{[(\Delta P / \Delta z)_d - (\Delta P / \Delta z)_d^0] / g}{(\rho_g - \rho_l) - (\Delta P / \Delta z)_d^0 / g} \quad (6)$$

Equation (6) was used to evaluate the gas holdup of high-pressure slurry bubble columns because of its two advantages. The solids density,  $\rho_s$ , cannot be easily be measured for porous particles in liquids, as hydrocarbon liquids can partially fill the pores of particles. Eq.(6) eliminates the particle density from the calculation. This technique can also determine if the particles in the column are completely suspended by comparing the dynamic pressure gradient at the gas-free suspension stage,  $(\Delta P / \Delta z)_d^0$ , obtained at different gas velocities.  $(\Delta P / \Delta z)_d^0$  remains a constant when all the particles are suspended. In the literature, sampling of the liquid-solid mixture has been used for the same purpose. However, the sampling technique at high pressures is tedious and inconvenient to conduct. Also, the amount of liquid and particles cannot be maintained constant.

Figure 4 shows the gas holdup in a slurry bubble column with a solids concentration of 20 wt % at 28°C and various pressures. It can be seen that the gas holdup increases with an increase in pressure. The difference between this result and that obtained by sampling of liquid-solid mixture is negligible.

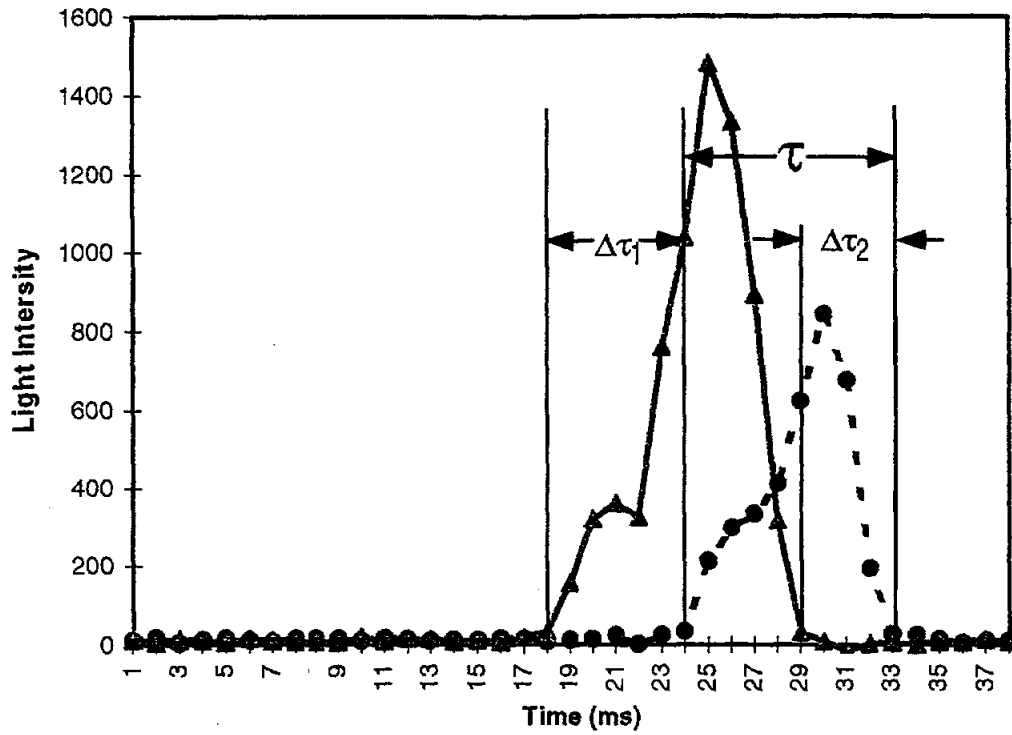


Figure 1. Characteristics and Notations of Peaks of Light Intensity Signals

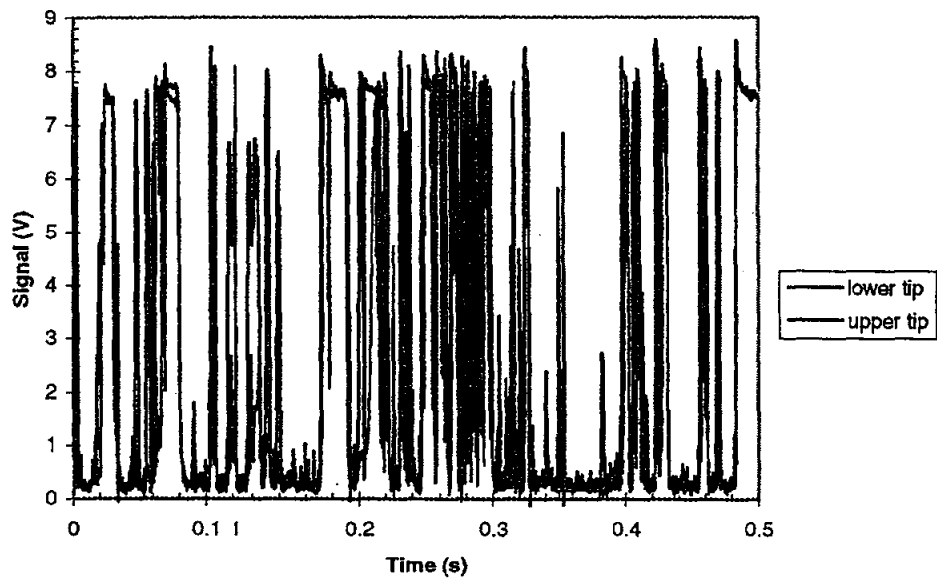
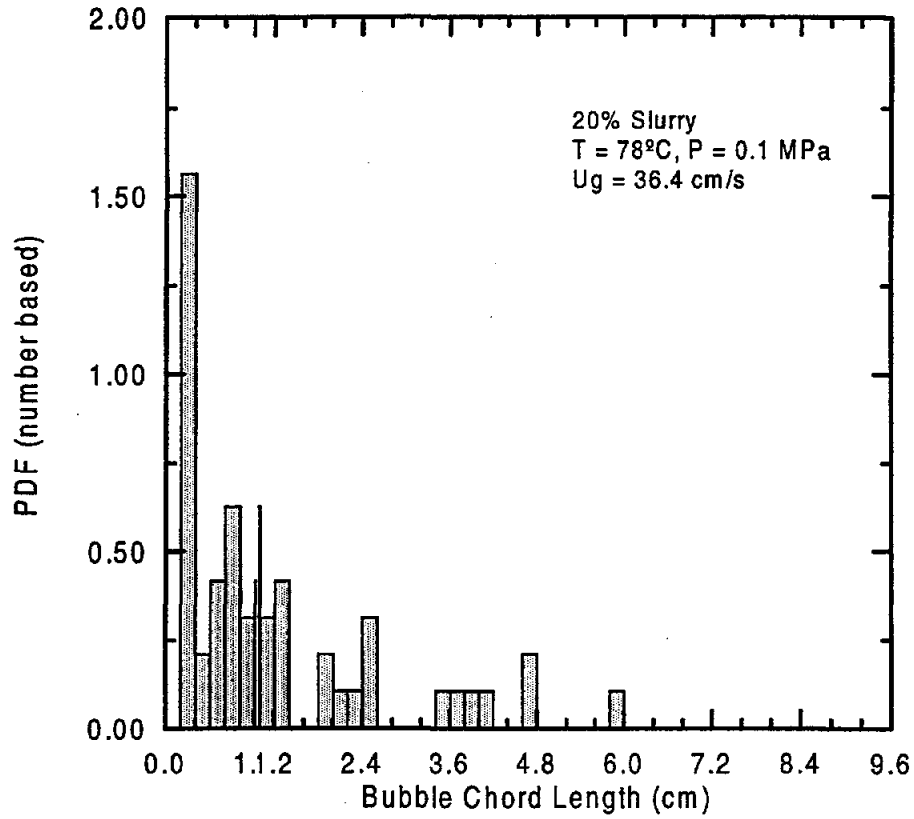
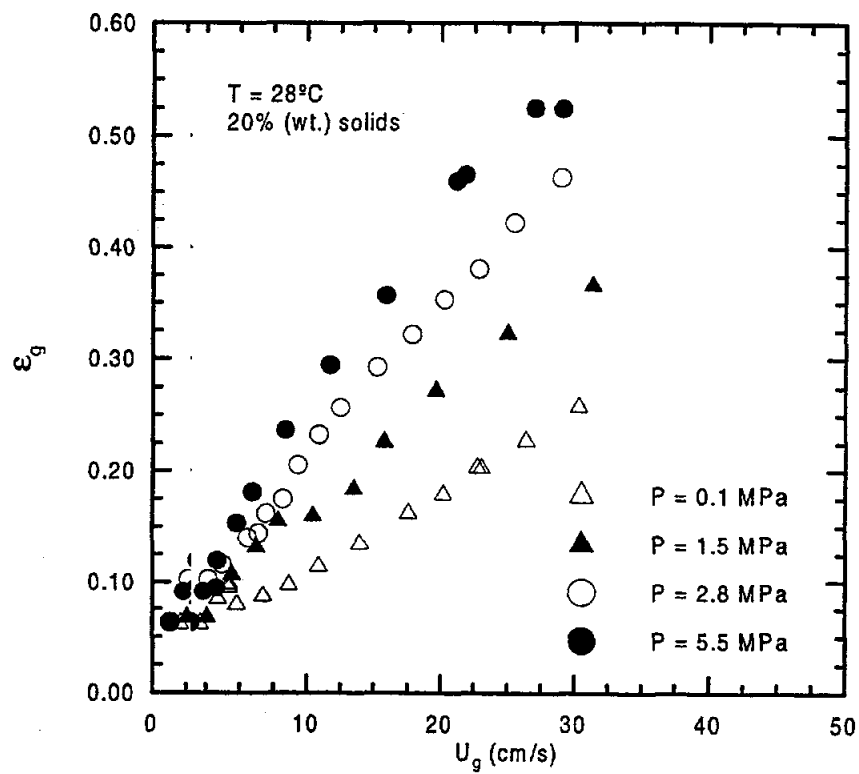


Figure 2. Typical Signals Obtained in Slurry Bubble Column



**Figure 3. A Typical Bubble Chord Length Distribution from the Computer Code**



**Figure 4. Gas Holdup in a Slurry Bubble Column at 28°C and Various Pressures**

**NOVEL TECHNIQUES FOR SLURRY BUBBLE COLUMN HYDRODYNAMICS**

**First Annual Report for Grant DE-FG 22-95 PC 95212**

**July 1, 1996**

**SECTION IV: REPORT FROM OHIO STATE UNIVERSITY  
(HEAT TRANSFER MEASUREMENTS)**

L.S. Fan, S. Kumar, D.J. Lee, P. Jiang, J. Reese  
Department of Chemical Engineering  
The Ohio State University  
Columbus, Ohio 43210



## **OBJECTIVE**

A special heat transfer probe is developed which is used to measure instantaneous local heat transfer coefficients due to the passage of single gas bubbles injected in liquid and liquid-solid systems. Also the reliability and accuracy of the probe are validated.

## **INTRODUCTION**

High heat transfer rate is one of the most important characteristics in the operation of a slurry bubble column which results in effective reaction temperature control in such reactors. Fundamental heat transfer studies have been concerned mainly with the measurement of time-averaged heat transfer from the column wall to the bed and/or from the surface of immersed heating object to the bed under steady state conditions. Due to inherent complexity of multiphase flow systems, however, little has been known in the past about the intrinsic mechanism underlying the enhanced heat transfer in bubbling systems over non-bubbling systems. Therefore, a better understanding of the heat transfer behavior and the underlying mechanism is essential for the design, control, and optimum operation of such reactors.

The heat transfer property in the bed is intimately associated with the bubble motion, bubble size, and phase holdups which are affected by fluid flow including wake flow. The wake flow behavior, such as temporal variations in the shear flow at the bubble edge, chaotic primary wake, and vortex-vortex interaction, differs distinctively from the fluid flow behavior in the bulk region (Fan and Tsuchiya, 1990). Thus, a fundamental understanding of bubble-wake dynamics forms a necessary basis for a complete

description of various transport processes in these systems, and to predict fully the heat transfer performance of gas-liquid and gas-liquid-solid systems, effects of bubble wake need to be considered. The bubble wake effect on heat transfer can be quantified by the measurement of the instantaneous local changes in the heat transfer coefficient, which depends strongly on the local hydrodynamics of the bed.

The complex behavior of bubble columns is a direct result of the local flow structure which are time-variant due to the intrinsic dynamic behavior of the dispersed gas-phase motion and associated wake interaction. Therefore, to obtain a better understanding of the extremely complex flow structure in bubble columns and its effects on the pertinent hydrodynamic properties and heat transfer characteristics, it is necessary to understand a simplified system involving a single bubble moving in liquid and liquid-solid systems.

To measure local instantaneous changes in heat transfer coefficients due to the passage of single gas bubble, a special heat transfer probe is developed. This report highlights the design of the novel heat transfer probe and its uniqueness and capability for accurately measuring the local instantaneous heat transfer coefficients in multiphase flow systems. Moreover, discussions of the mechanism of heat transfer enhancement due to the presence of bubble in simplified systems involving single bubble injection in liquid and liquid-solid systems is presented.

## EXPERIMENTAL

A schematic diagram of the experimental apparatus is shown in Fig. 1. The experiments are performed in a three-dimensional Plexiglas column, 150 cm high and 1.62 cm ID. Liquid enters the column through a packed layer of 6 mm glass beads and a perforated-plate distributor ensuring uniform distribution of liquid in the column. The support for the fluidized particles is provided by a 200-mesh wire cloth. A steady liquid velocity is maintained by circulating water through a reservoir and a rotary pump. Tap water is used as the liquid phase in the experiments. Fluidized particles used are 163  $\mu\text{m}$  (GB163) and 326  $\mu\text{m}$  (GBB326) glass beads. The physical properties of solid particles are given in Table 1.

Experiments involve single bubble injection in liquids and liquid-solid suspensions as shown in Figs. 2(a) and 2(b). A three-dimensional cup bubble injection system in Fig. 1 is designed in this study to introduce single bubbles without pressure perturbation or any satellites generation. A hemispherical cup of 2.5 cm diameter is inserted through the wall at 10 cm above the distributor. A known volume of air is injected into the cup through the stainless tube using a syringe. The trapped bubble is then released by turning the cup. The bubble volume varied from 3  $\text{cm}^3$  to 10  $\text{cm}^3$  with the corresponding bubble Reynolds number (based on equivalent bubble diameter)  $Re_b$ , ranging from 5,300 to 9,000. Under these values of  $Re_b$ , the bubble is of spherical cap shape and the wake configuration is symmetric along the vertical axis of bubble. Furthermore, the bubbles rose almost rectilinearly. Miyahara *et al.* (1988) reported that for  $Re_b$  beyond 5,000 the bubble tends to discharge vorticity symmetrically and rises rectilinearly.

## INSTANTANEOUS HEAT TRANSFER MEASUREMENT / PROBE DESIGN

The instantaneous local heat transfer rate is measured by a heat flow sensor/heater assembly (heat transfer probe). Figure 3 shows the details of the probe design. The probe assembly consists of five components; microfoil heat flow sensor, copper plate, foil heater, thermosetting material (insulator), and support. The foil heater is 2.54 cm high and 1.91 cm wide, and is heated by a constant voltage DC power source.

The local heat flux is measured directly by a microfoil differential heat-flow sensor (RdF corporation, Model 204453-1; Table 2). The overall dimension of the sensor is 1.27 cm  $\times$  1.27 cm  $\times$  0.008 cm. This sensor utilizes thin foil type thermopile bonded to both sides of a known thermal barrier (Fig. 4). The difference in temperature across the thermal barrier known, the sensor is factory-calibrated to provide the relation between the sensor output (voltage) and the local heat flux (Fig. 5). The unique construction of the sensor provides it with low thermal capacitance ( $204.41 \text{ J}\cdot\text{m}^{-2}/\text{K}$ ), low thermal impedance ( $5.28 \times 10^{-4} \text{ m}^2\cdot\text{K}/\text{W}$ ), high sensitivity ( $8.56 \times 10^{-3} \mu\text{V}/\text{W}\cdot\text{m}^{-2}$ ), fast response time (0.02 s), and minimal thermal perturbation to the heat flow. The microfoil heat flow sensor is flush mounted on the copper plate which is attached to the micro-foil heater and insulator as shown in Fig. 3.

The sensor can accurately measure the heat flux and its surface temperature over a small surface area. The heater/sensor probe assembly is usually positioned in the center of the column with the help of a support as shown in Fig. 1. Due to the rectilinear motion of bubbles, there is a high probability of bubbles striking the probe surface or at least passing very close to it. The probe is located at about 50 cm from the point of bubble injection,

which allows sufficient distance for the bubble to reach its terminal velocity (Miyahara *et al.*, 1988). Since the width of the probe at a horizontal section of the column is small (0.32 cm), the disturbance to the flow in the vicinity of the probe is minimal and the fluidized state remains relatively undisturbed. A sheathed copper-constantan thermocouple located at the column wall is used for the measurement of the bulk temperature. The average bulk temperature is also monitored by a digital thermometer.

## MEASUREMENT TECHNIQUE

Signals for the heat flux as well as the temperature difference between the probe surface and bulk are sampled simultaneously at the rate of 186.2 Hz for 11 seconds. The signals from the sensor (typically in microvolt range) are amplified to millivolts range by the amplifier/multiplexer system (Metrabyte EXP-16) and interfaced with the high speed microcomputer data acquisition system (Metrabyte DASH-16). Digital signals stored in the computer are converted to the corresponding heat transfer rate and the temperature difference using proper calibration.

To reduce the high frequency noise in the original signal, software signal processing is performed. The signals are smoothed by employing a low-pass filter and the computations are performed using Fast Fourier Transforms. A typical raw and filtered signal of the temperature difference  $\Delta T_i (= T_{si} - T_{\infty})$  for a signal bubble injection in a liquid-solid fluidized bed containing GB163 is shown in Fig. 6. There is a significant change in temperature difference due to the passage of bubble, but the change in  $q_i$  is not so significant compared to the temperature difference. Also, there is a large fluctuation in  $q_i$

as compared to  $\Delta T_i$ . Since the change in the instantaneous heat transfer rate depends on many factors including the thermal balance on both sides of the heater, the instantaneous heat transfer coefficient,  $h_i$ , is obtained from the instantaneous change in the temperature difference,  $\Delta T_i$ , and the time averaged heat transfer rate,  $Q$ .

$$h_i = \frac{Q}{\Delta T_i} \quad (1)$$

Typical differential temperature  $\Delta T_i$  in the stagnant liquid medium is 10°C, while that in the bubble column is 4°C. Due to the small dimension of the probe and minimal alteration in the hydrodynamic condition near the heat transfer surface, the measured instantaneous heat transfer coefficient in Eq. (1) is a direct measure of the local instantaneous heat transfer coefficients in the bed at that particular location. The local time-averaged heat transfer coefficient can be obtained by averaging the instantaneous heat transfer coefficient data over a number of sampling points (2048) as

$$h_w = \frac{1}{n} \sum_{i=1}^n \frac{Q}{\Delta T_i} \quad (2)$$

The small dimension of the probe (20 to 30 times smaller heat transfer area compared to conventional probes employed by Baker *et al.*, 1978 and Magliotou *et al.*, 1988), ease of installation, and high accuracy in measurements render its application limitless. For example, the probe could easily be positioned at any location in the bed to measure the instantaneous and time-averaged heat transfer coefficient. Also, since the heat transfer measurements are local in nature, the probe may be used for locating in-bed non homogeneity in a multiphase flow system. Thus, the probe is capable of instantaneous and local hydrodynamic characterization of a particulate multiphase reactor, thereby

providing significant information regarding the radial and axial variation of heat transfer in an industrial and pilot size reactor which would be of enormous practical significance in better design and control of such systems.

## PROBE VALIDATION

The reliability and accuracy of the probe are validated by performing heat transfer measurements in liquid (water) systems and liquid-solid fluidized beds. Time-averaged local heat transfer coefficients in liquid-solid fluidized beds agree well with the immersed object-to-bed heat transfer coefficients data and correlations reported in the literature (e.g., Baker *et al.*, 1978 and Kato *et al.*, 1984). Also, a good agreement is obtained between the measured heat transfer coefficient in stationary water with that predicted by the heat transfer correlation for laminar free convection on a vertical plate immersed in stationary water reported in the literature (e.g., Incropera and De Witt, 1985).

## INSTANTANEOUS HEAT TRANSFER COEFFICIENT

Figures 7, 8, and 9 show the instantaneous heat transfer coefficient due to the passage of a single gas bubble in liquid, in liquid-solid systems containing GB163, and in liquid-solid systems containing GB326, respectively. The instantaneous heat transfer coefficient increased rapidly, attained a maximum value, and then gradually recovered to the initial value in liquid and liquid-solid systems. It should also be noted from Figs. 7, 8, and 9 that due to the presence of secondary wake in liquid and liquid-solid systems, the heat transfer coefficient does not completely recover to the baseline value within the

sampling time of around 11 s. The effect of single bubble injection on heat transfer enhancement in the liquid system lasts much longer than in liquid-solid systems. Larger primary and secondary wakes and stronger vortex in such systems are primarily responsible for this phenomenon. All figures show that increased bubble volume  $V_b$  causes increased enhancement due to larger bubble wake and stronger vortices.

Particle sizes in liquid-solid systems affect the bubble-wake induced heat transfer enhancement. In Figs. 8 a and 9, heterogeneous effects caused by the larger particle size reduce the bubble-wake induced enhancement in heat transfer although the baseline value is increased. The baseline  $\alpha$  values (time-averaged heat transfer coefficient with no bubble injection) for liquid is  $2855 \text{ W/m}^2\cdot\text{K}$ , for GB163 system is  $808 \text{ W/m}^2\cdot\text{K}$ , and for GB326 system is  $815 \text{ W/m}^2\cdot\text{K}$ .

## CONCLUDING REMARKS

A novel heat transfer probe is developed which accurately measured the instantaneous changes in heat transfer due to the passage of single gas bubble in liquid and liquid-solid systems. For a bubble passing through the probe, the maximum heat transfer is observed in the wake region at a short distance behind the bubble in the upward flow of fluid rising along the wake central axis.

In both liquid and liquid-solid systems, the observed local maximum in the heat transfer coefficient behind a rising bubble is due to the effect of bubble wake. The local maximum in heat transfer, however, is more pronounced in liquid than in liquid-solid



systems. Also, the heat transfer enhancement due to the bubble passage increases with the bubble size due to larger bubble wake and stronger vortices.

## NOMENCLATURE

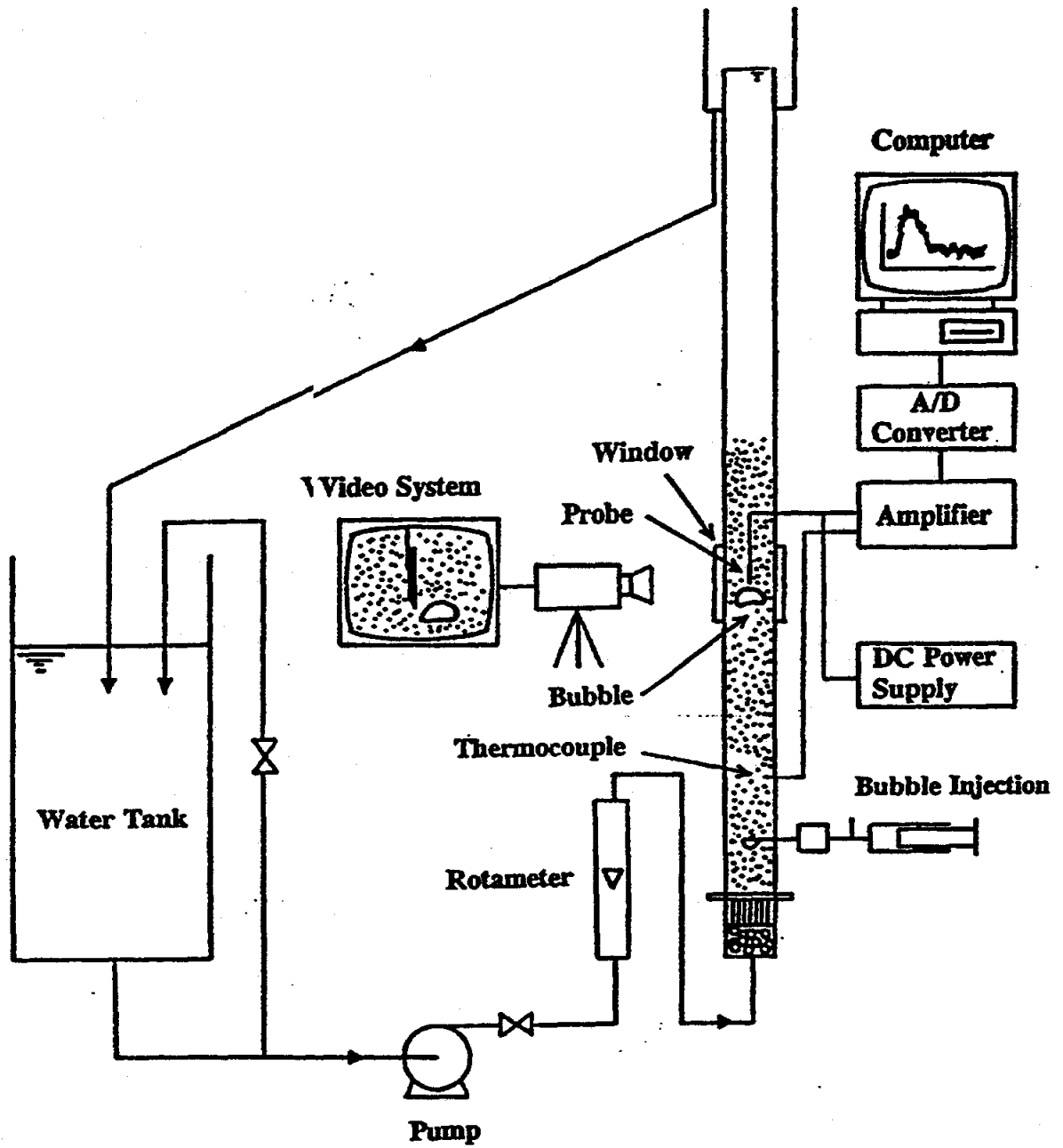
- $h_{av}$  time-averaged heat transfer coefficient over the sampling time,  $W/m^2 \cdot K$
- $h_i$  instantaneous heat transfer coefficient,  $W/m^2 \cdot K$
- $n$  number of sampling points, 2048
- $Q$  time-averaged heat flux,  $W/m^2$
- $V_b$  bubble volume,  $cm^3$
- $\Delta T_i$  instantaneous temperature difference between the probe surface ( $T_{st}$ ) and bulk ( $T_{\infty}$ ), K

## REFERENCES

- C. G. J. Baker, E. R. Armstrong, and M. A. Bergougnou, "Heat Transfer in Three-Phase Fluidized Beds," *Power Technology*, 21, 195 (1978).
- L.-S. Fan and K. Tsuchiya, *Bubble Wake Dynamics in Liquids and Liquid-Solid Suspensions*, Butterworth-Heinemann, Stoneham, MA (1990).
- F. P. Incropera and D. P. De Witt, *Introduction to Heat Transfer*, 392, Wiley, NY (1985).
- Y. Kato, Y. Taura, T. Kago, and S. Morooka, "Heat Transfer Coefficient Between an Inserted Vertical Tube and a Three-Phase Fluidized Bed," *Kagaku Kogaku Ronbunshu*, 10, 427 (1984).
- M. Magiliotou, Y.-M. Chen, and L.-S. Fan, "Bed-Immersed Object Heat Transfer in a Three-Phase Fluidized Bed," *AIChE J.*, 34, 1043 (1988).
- T. Miyahara, K. Tsuchiya, and L.-S. Fan, "Wake Properties of a Single Gas Bubble in a Three-Dimensional Liquid-Solid Fluidized Bed," *Int. J. Multiphase Flow*, 14, 749 (1988).

## FIGURES AND TABLES

- Figure 1      A schematic of experimental setup.
- Figure 2      A schematic of experimental conditions.
- Figure 3      Heat-transfer probe design.
- Figure 4      A schematic of heat flow sensor.
- Figure 5      Heat flow sensor calibration.
- Figure 6      A typical raw and processed signal.
- Figure 7      Effects of bubble size on instantaneous heat-transfer coefficient due to the passage of bubble in liquid for probe located at the center of column.
- Figure 8      Effects of bubble size on instantaneous heat-transfer coefficient due to the passage of bubble in liquid-solid fluidized bed with GB163 for probe located at the center of column.
- Figure 9      Effects of bubble size on instantaneous heat-transfer coefficient due to the passage of bubble in liquid-solid fluidized bed with GB326 for probe located at the center of column.
- Table 1      Physical properties of spherical particles.
- Table 2      Types of microfoil heat flow sensor.



**Figure 1** A schematic of experimental setup.

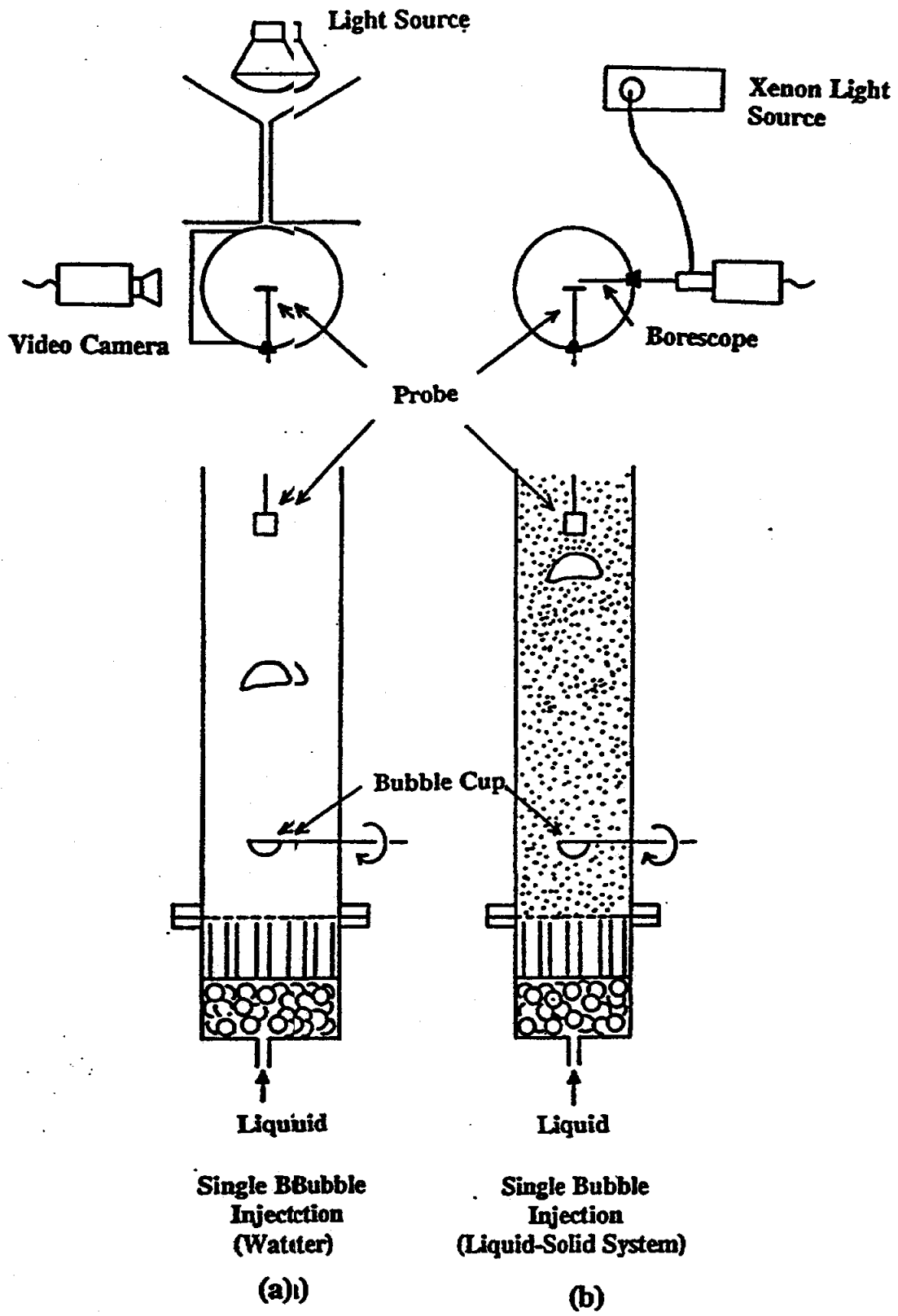
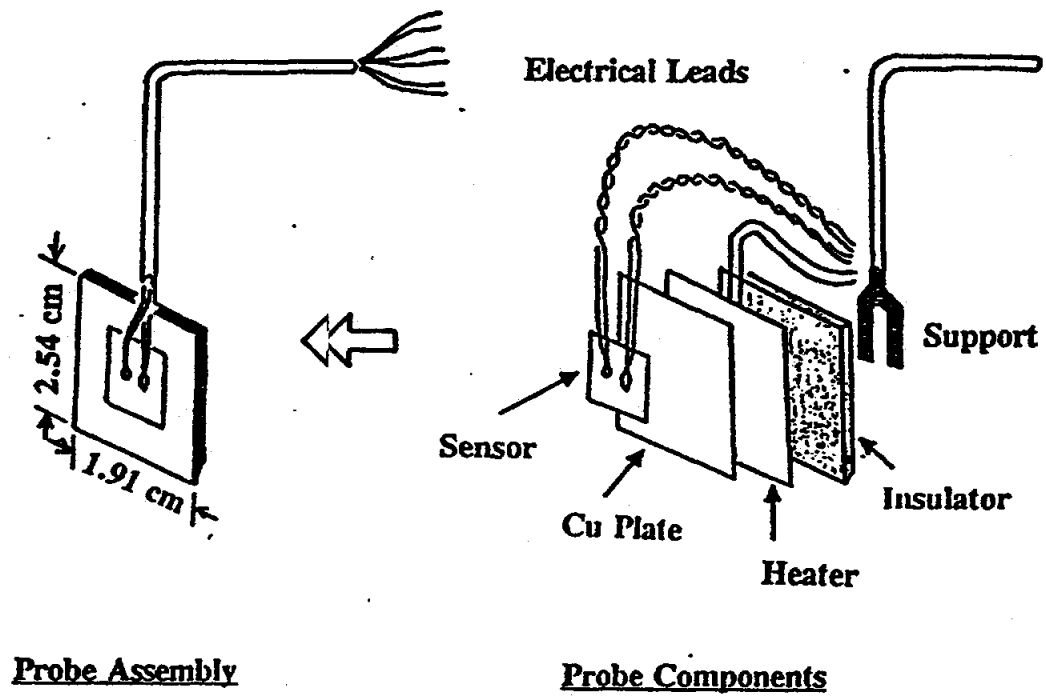
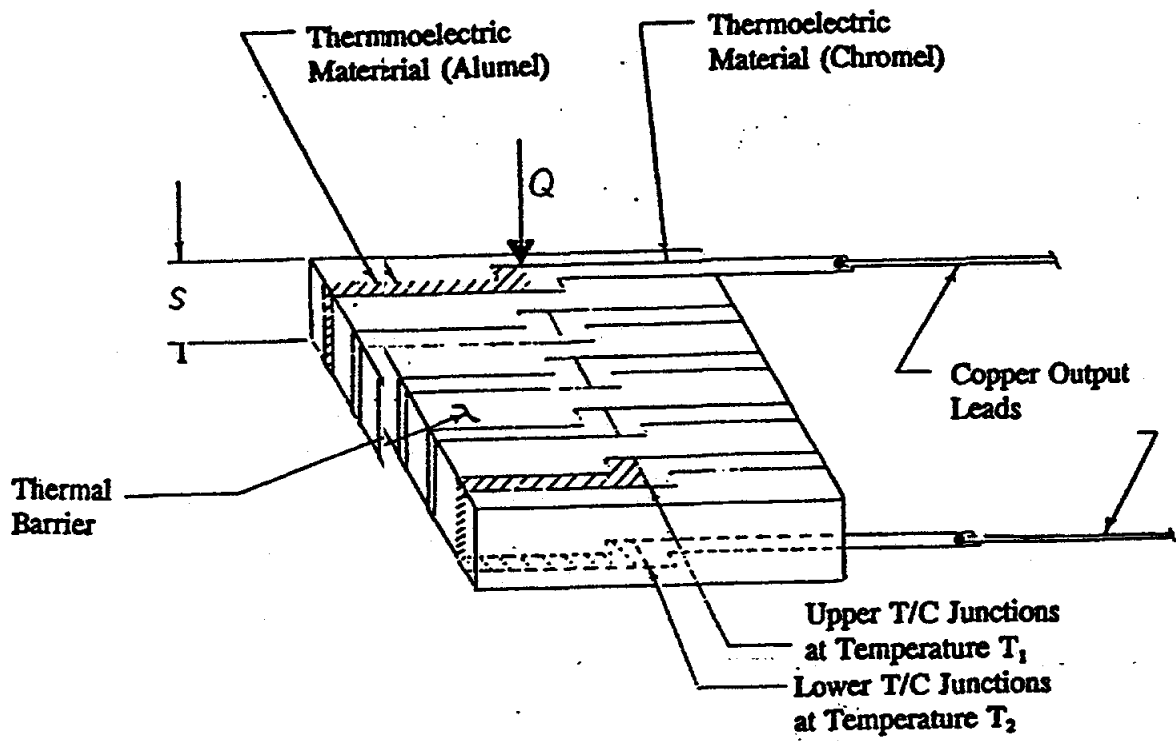


Figure 2 A schematic of experimental conditions.



**Figure 3 Heat-transfer probe design.**



**Figure 4** A schematic of heat flow sensor.

Heat Flow Sensor Output at 70°F =  $8.24 \times 10^{-3} \mu\text{V/W.m}^2$

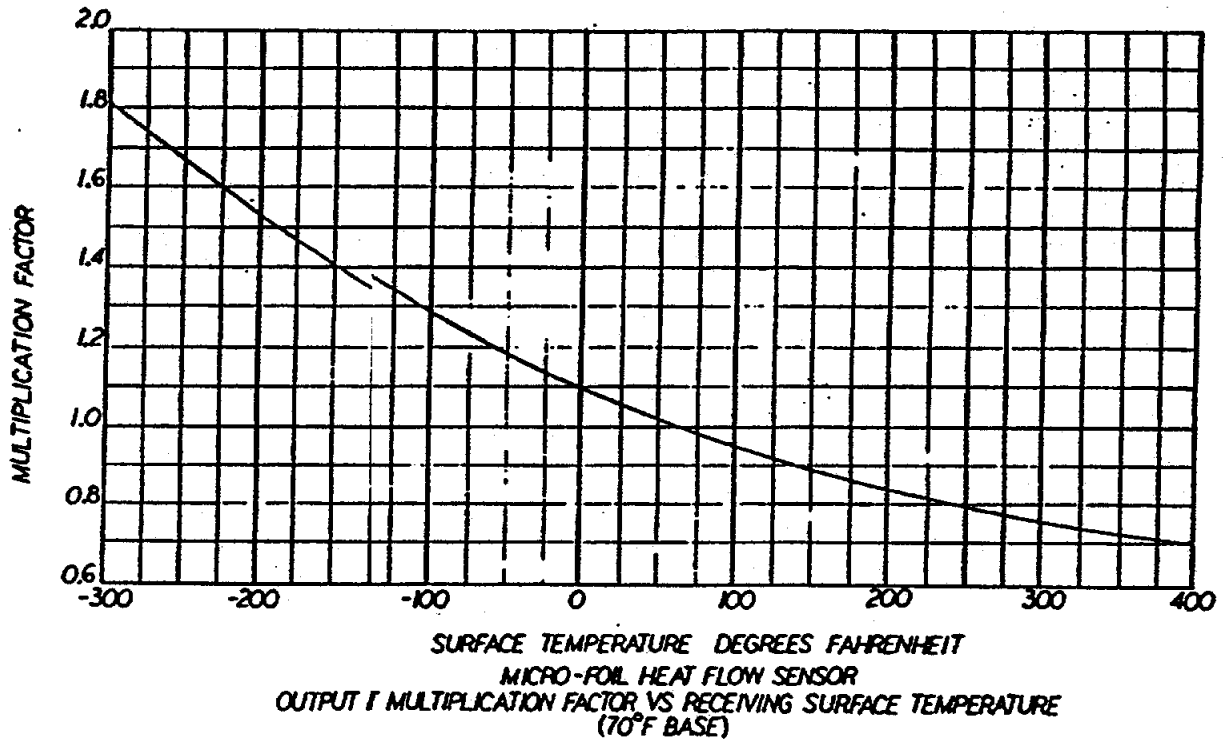
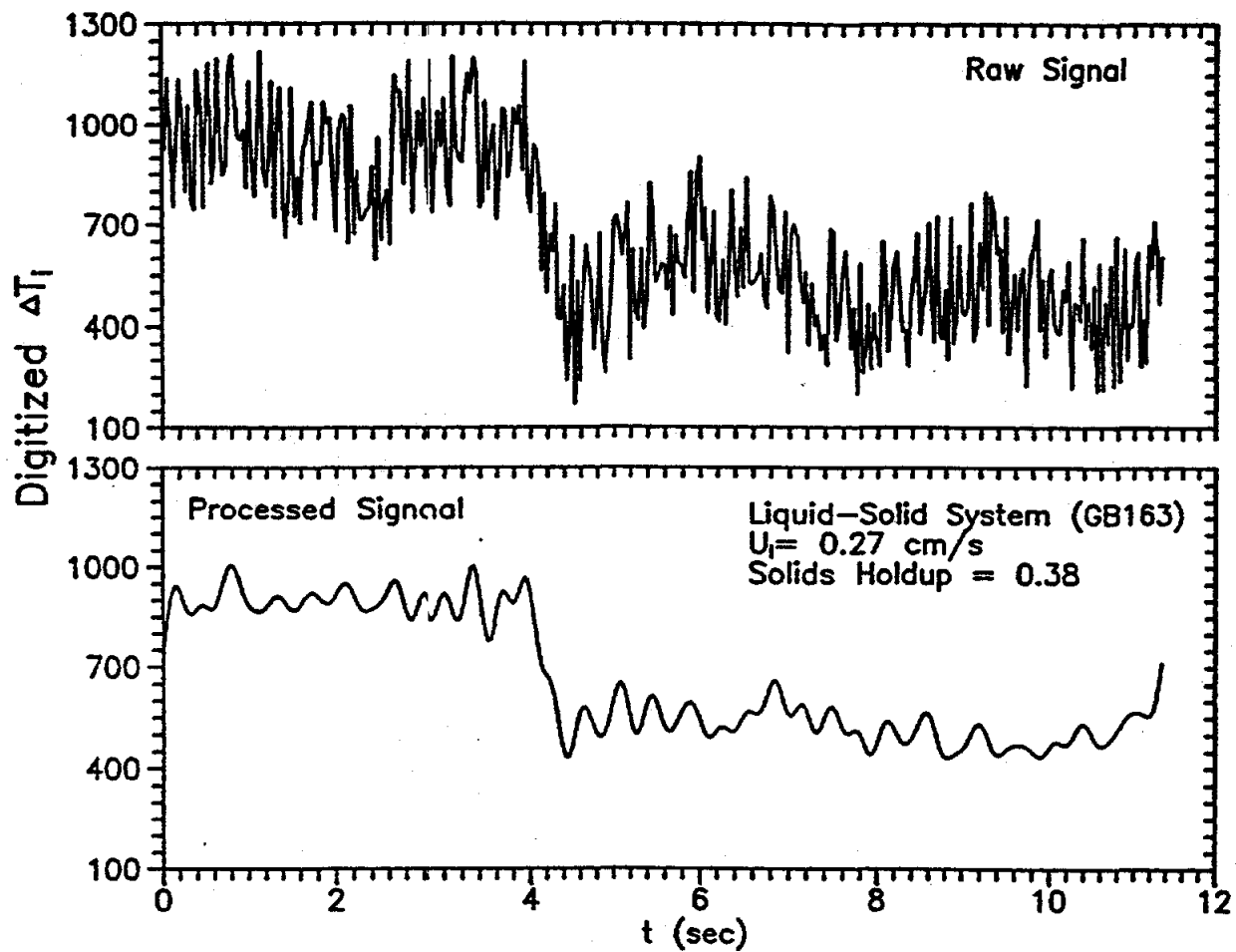
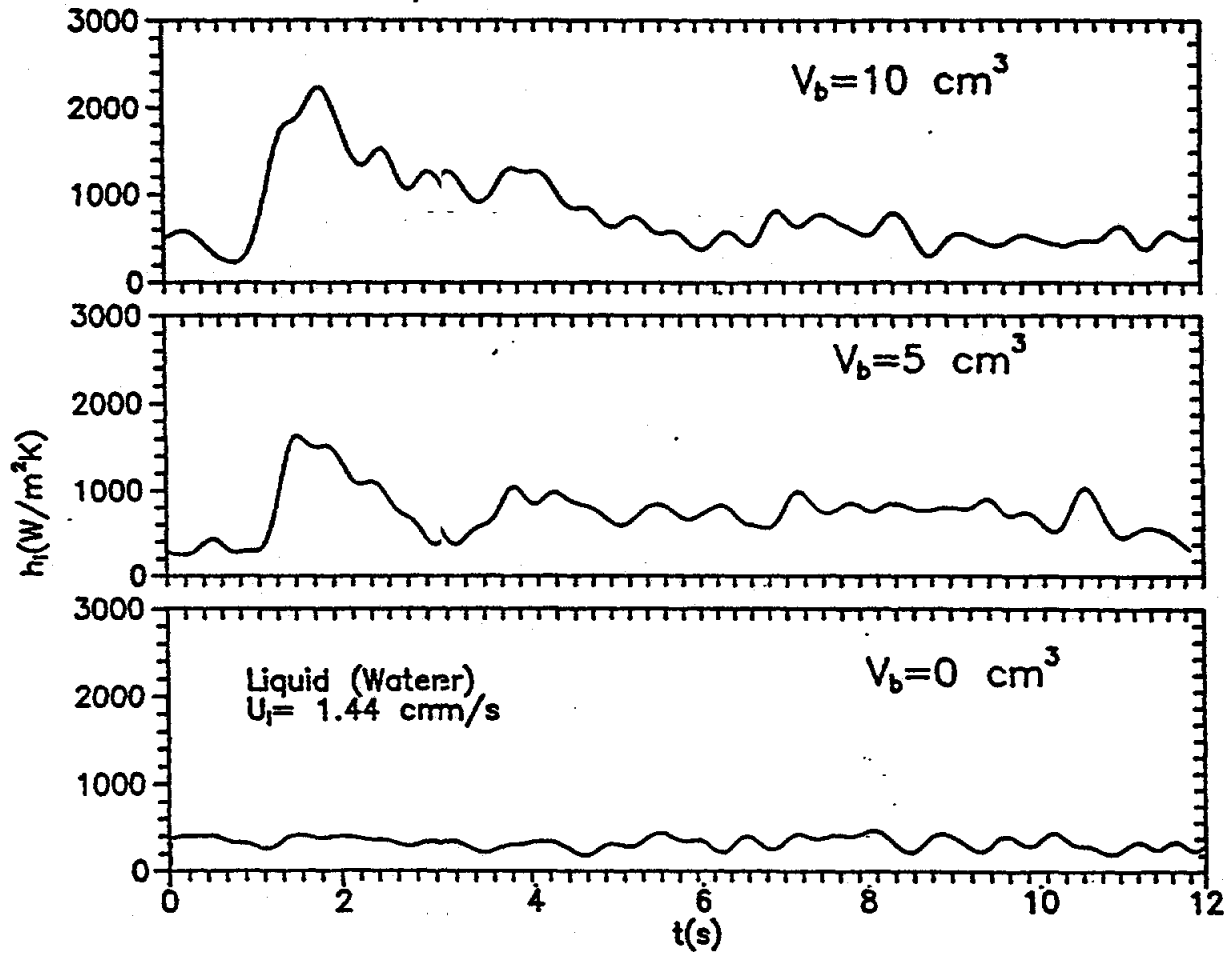


Figure 5 Heat flow sensor calibration.

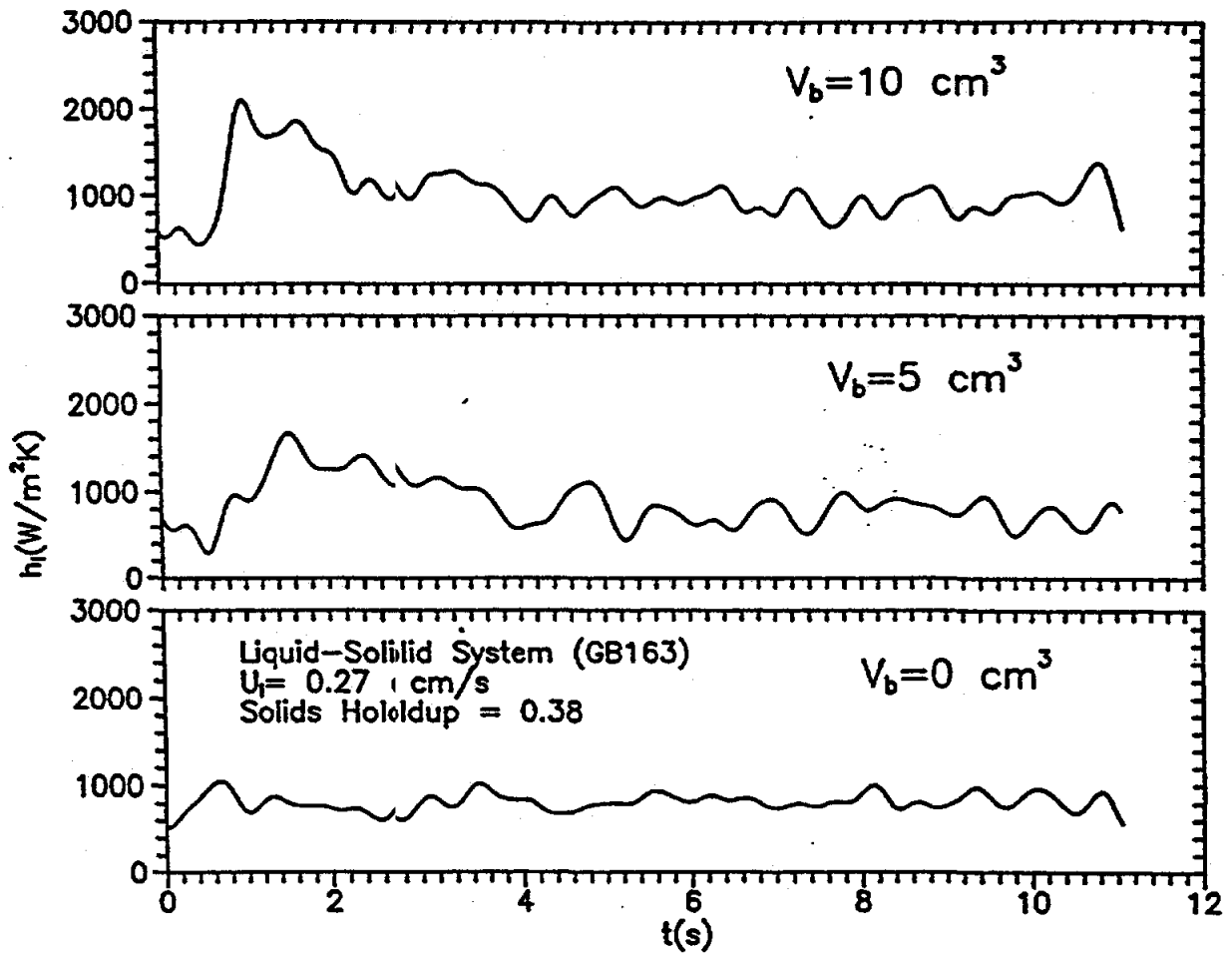


**Figure 6** A typical raw and processed signal.

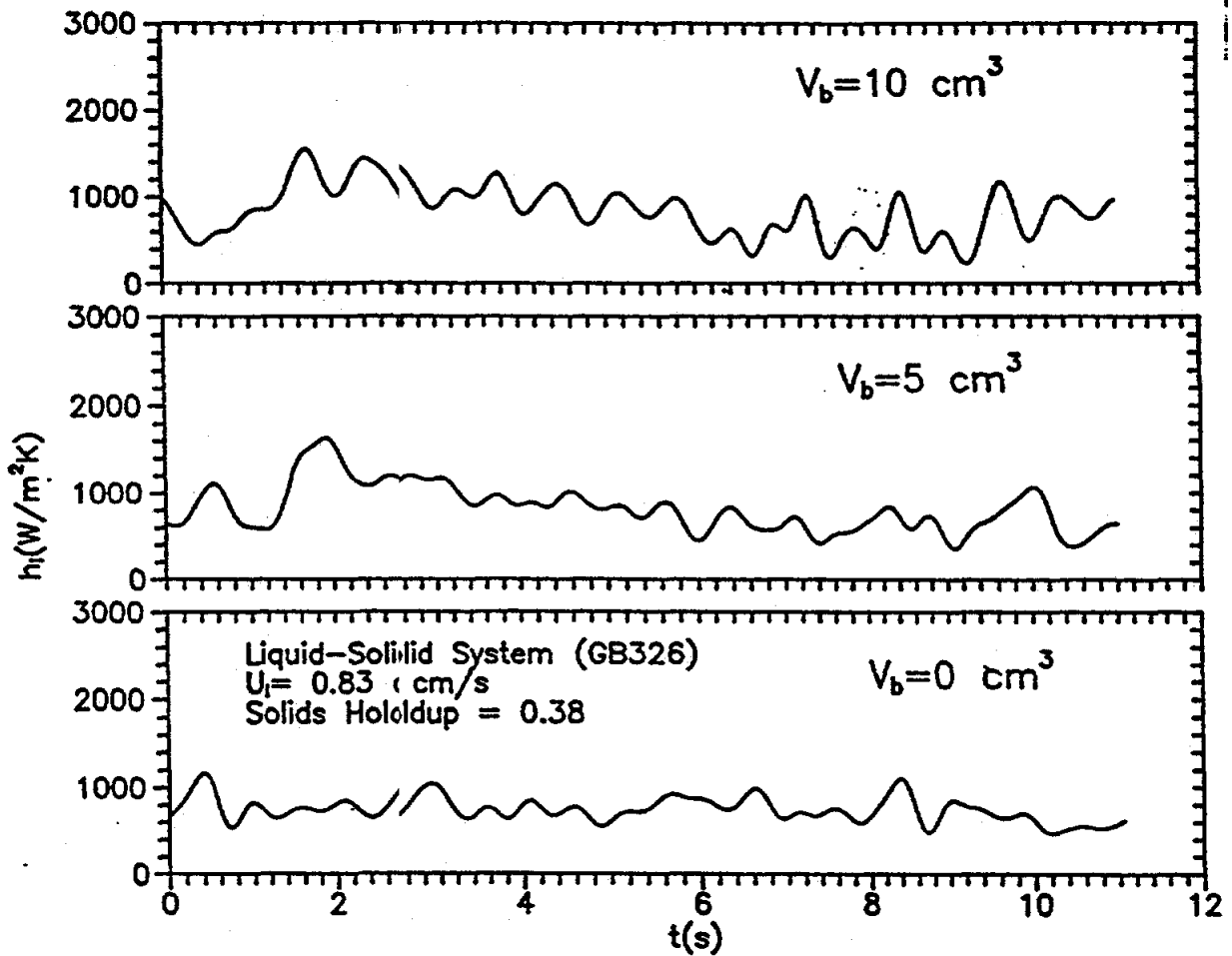




**Figure 7** Effects of bubble size on instantaneous heat-transfer coefficient due to the passage of a bubble in liquid for probe located at the center of column.



**Figure 8** Effects of bubble size on instantaneous heat-transfer coefficient due to the passage of bubble in liquid-solid fluidized bed with GB163 for probe located at the center of column.



**Figure 9** Effects of bubble size on instantaneous heat-transfer coefficient due to the passage of bubble in liquid-solid fluidized bed with GB326 for probe located at the center of column.

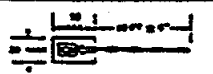
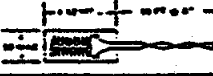
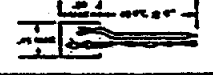
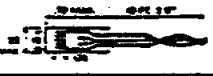
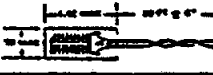

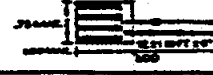
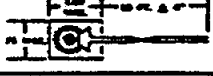
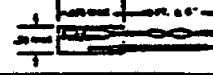

**Table 1**      **Physical properties of spherical particles.**

| Particle   | Notation | Average diameter (mm) | Density (g/cm <sup>3</sup> ) | $\epsilon_o^a$ | $U_t^b$ (m/s)        |
|------------|----------|-----------------------|------------------------------|----------------|----------------------|
| Glass bead | GB163    | 0.163                 | 2.50                         | 0.63           | $1.7 \times 10^{-2}$ |
| Glass bead | GB326    | 0.326                 | 2.50                         | 0.62           | $4.4 \times 10^{-2}$ |

<sup>a</sup>Packed bed solids fraction

<sup>b</sup>Fan and Tsuchiya (1990)

Table 2 Types of microfoil heat flow sensor.

| CONFIGURATION*  | Part Number | Nominal Sensitivity<br>( $\mu\text{V}/\text{Btu}/\text{ft}^2\text{-hr.}$ ) | Maximum Recommended Heat Flux<br>( $\text{Btu}/\text{ft}^2\text{-Sec.}$ ) | Response Time<br>(Seconds) | Sensor Resistance<br>( $\Omega$ Max.) | Maximum Operating Temp. ( $^{\circ}\text{F}$ ) | Nominal Thickness<br>in (inches) | Thermal Properties  |  |
|---|-------------|--|---|----------------------------|---------------------------------------|--|----------------------------------|---|--|
|   |             |  |   |                            |                                       |  |                                  | Capacitance<br>$\text{Btu}/\text{ft}^2\text{-}^{\circ}\text{F}$ | Impedance<br>$^{\circ}\text{F}$ per $\text{ft}^2\text{-hr.}$ |
|    | 2040450-1   | 0.02   | 50  | .020                       | 5                                     | 300  | .003                             | .01   | .003   |
|   | 2040450-2   | 0.06   | 25  | .060                       | 5                                     | 300  | .005                             | .02   | .005   |
|   | 2040450-3   | 0.2  | 10  | .400                       | 5                                     | 300  | .012                             | .05   | .012   |
|    | 2040452-1   | 0.2  | 50  | .020                       | 20                                    | 300  | .003                             | .01   | .003   |
|   | 2040452-2   | 0.6  | 25  | .060                       | 20                                    | 300  | .005                             | .02   | .005   |
|   | 2040452-3   | 2.0  | 10  | .400                       | 20                                    | 300  | .012                             | .05   | .012   |
|    | 2040453-1   | 0.02   | 50  | .020                       | 5                                     | 300  | .003                             | .01   | .003   |
|   | 2040453-2   | 0.06   | 25  | .060                       | 5                                     | 300  | .005                             | .02   | .005   |
|   | 2040453-3   | 0.2  | 10  | .400                       | 5                                     | 300  | .012                             | .05   | .012   |
|    | 2707036-1   | 0.1  | 50  | .020                       | 10                                    | 300  | .003                             | .01   | .003   |
|   | 2707036-2   | 0.3  | 25  | .060                       | 10                                    | 300  | .005                             | .02   | .005   |
|   | 2707036-3   | 1.0  | 10  | .400                       | 10                                    | 300  | .012                             | .05   | .012   |
|   | 2040455-1   | 0.2  | 50  | .020                       | 20                                    | 300  | .003                             | .01   | .003   |
|   | 2040455-2   | 0.6  | 25  | .060                       | 20                                    | 300  | .005                             | .02   | .005   |
|   | 2040455-3   | 2.0  | 10  | .400                       | 20                                    | 300  | .012                             | .05   | .012   |
|  | 2040456-1   | 1.1  | 50  | .020                       | 100                                   | 300  | .004                             | .01   | .003   |
|   | 2040456-2   | 3.3  | 25  | .060                       | 100                                   | 300  | .006                             | .02   | .005   |
|   | 2040456-3   | 11.0   | 10  | .400                       | 100                                   | 300  | .013                             | .05   | .012   |
|  | 2040457-1   | 1.1  | 50  | .020                       | 100                                   | 300  | .004                             | .01   | .003   |
|   | 2040457-2   | 3.3  | 25  | .060                       | 100                                   | 300  | .006                             | .02   | .005   |
|   | 2040457-3   | 11.0   | 10  | .400                       | 100                                   | 300  | .013                             | .05   | .012   |
|  | 2040466-1   | 0.2  | 50  | .020                       | 15                                    | 300  | .003                             | .01   | .003   |
|   | 2040466-2   | 0.6  | 25  | .060                       | 15                                    | 300  | .005                             | .02   | .005   |
|   | 2040466-3   | 2.2  | 10  | .400                       | 15                                    | 300  | .012                             | .05   | .012   |
|  | 2040472-1   | 0.2  | 50  | .020                       | 30                                    | 300  | .003                             | .01   | .003   |
|   | 2040472-2   | 0.6  | 25  | .060                       | 30                                    | 300  | .005                             | .02   | .005   |
|   | 2040472-3   | 2.0  | 10  | .400                       | 30                                    | 300  | .012                             | .05   | .012   |
|  | 2040480-1   | 0.2  | 50  | .020                       | 20                                    | 300  | .005                             | .01   | .003   |
|   | 2040480-2   | 0.6  | 25  | .060                       | 20                                    | 300  | .005                             | .02   | .005   |
|   | 2040480-3   | 2.0  | 10  | .400                       | 20                                    | 300  | .005                             | .05   | .012   |